# Wave instability induced by nonlocal spatial coupling in a model of the light-sensitive Belousov-Zhabotinsky reaction

Ernesto M. Nicola,[1,2,*] Markus Bär,[3] and Harald Engel[1,†]
[1]*Institut für Theoretische Physik, Technische Universität Berlin, PN 7-1 Hardenbergstraße 36, D-10623 Berlin, Germany*
[2]*Theoretische Physik II, Physikalisches Institut, Universität Bayreuth, D-95440 Bayreuth, Germany*
[3]*Physikalisch-Technische Bundesanstalt, Fachbereich 8.4, Abbestraße 2-12, D-10587 Berlin, Germany*
(Received 6 January 2006; published 28 June 2006)

We study spatiotemporal patterns resulting from instabilities induced by nonlocal spatial coupling in the Oregonator model of the light-sensitive Belousov-Zhabotinsky reaction. In this system, nonlocal coupling can be externally imposed by means of an optical feedback loop which links the intensity of locally applied illumination with the activity in a certain vicinity of a particular point weighted by a given coupling function. This effect is included in the three-variable Oregonator model by an additional integral term in the photochemically induced bromide flow. A linear stability analysis of this modified Oregonator model predicts that wave and Turing instabilities of the homogeneous steady state can be induced for experimentally realistic parameter values. In particular, we find that a long-range inhibition in the optical feedback leads to a Turing instability, while a long-range activation induces wave patterns. Using a weakly nonlinear analysis, we derive amplitude equations for the wave instability which are valid close to the instability threshold. Therein, we find that the wave instability occurs supercritically or subcritically and that traveling waves are preferred over standing waves. The results of the theoretical analysis are in good agreement with numerical simulations of the model near the wave instability threshold. For larger distances from threshold, a secondary breathing instability is found for traveling waves.

DOI: 10.1103/PhysRevE.73.066225 PACS number(s): 05.45.−a, 04.30.Nk, 05.65.+b, 82.30.Vy

## I. INTRODUCTION

The interplay between nonlinear local kinetics (bistable, excitable, or oscillatory) and short-range spatial coupling in reaction-diffusion systems is the origin of a large variety of spontaneously formed spatiotemporal patterns. Many different patterns such as traveling fronts, solitary pulses, periodic pulse trains, spiral waves, and spatiotemporal chaos have been observed [1,2]. On the other hand, long-range spatial communication arises naturally in various systems. The existence of this nonlocal coupling can significantly enlarge the spectrum of emerging patterns. Examples of nonlinear systems with nonlocal spatial coupling can be found in many different fields. They include electrochemical systems [3–5], neural tissue [6], chemical reactions [7,8], amplitude equations with nonlocal terms [9,10], and models of population dynamics [11–14].

In electrochemical systems, nonlocal coupling is mediated by the electric field in the electrolyte and gives rise to unexpected phenomena such as remote triggering of activation fronts [3], Turing-type patterns [4], and asymmetric standing waves [5]. Neural tissue provides a further example of long-range spatial communication as axons connect neurons over large distances [6]. Recently, a generic reaction-diffusion system with nonlocal spatial coupling was analyzed in [8]. Here the nonlocal coupling results from the adiabatic elimination of a fast variable. As a consequence of this nonlocal coupling, moving localized patches of traveling wave patterns embedded in a stationary Turing pattern background (and vice versa) have been observed [8].

Sometimes, the range of nonlocal coupling is very large and corresponds practically to global coupling. Intensively studied examples of such systems are catalytic surface reactions as, for example, the CO oxidation on Pt(110) single crystal surfaces under ultrahigh vacuum conditions [15–17]. Because the mean free path of the CO molecules in the gas phase is much larger than the size of the reaction chamber, a local perturbation in the CO partial pressure caused by adsorption of a CO molecule will be immediately spread out over the whole surface. This intrinsic global coupling through the gas phase has been shown to induce cluster and wave instabilities [16] and to be very useful in controlling spatiotemporal chaotic states [17].

In this paper we want to consider the effects of nonlocal spatial coupling in a realistic model for a chemical reaction. One of the best studied examples of chemical pattern formation is certainly the Belousov-Zhabotinsky (BZ) reaction [18,19]. After the pioneering work of Kuhnert in 1986 [20], a modification of the classical reaction that uses the light-sensitive complex Ruthenium-4,4′-dimethyl-2,2′-bipyridyl [further abbreviated as $Ru(dmbpy)_3^{2+}$] as redox catalyst, has attracted much attention. In the modified reaction illumination with light (460 nm) results in the release of bromide via reduction of bromomalonic acid by the photochemically excited $Ru(dmbpy)_3^{2+}$ ion. Bromide is the inhibitor of the reaction that controls the excitability of the system. Therefore, the light-sensitive variant of the BZ reaction offers the application of a wide variety of external perturbations to control pattern formation. It has been successfully employed in the periodic forcing of spiral waves in the excitable regime [21,22] and in resonant forcing of phase patterns under os-

*Present address: Max-Planck-Institut für Physik komplexer Systeme, Nöthnitzer Str. 38, D-01187 Dresden, Germany.
†Electronic address: h.engel@physik.tu-berlin.de

 

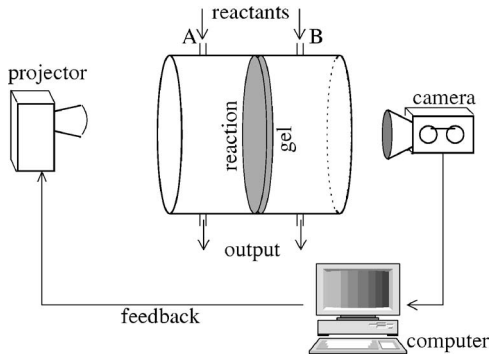


FIG. 1. Sketch of a possible experimental realization for nonlocal spatial coupling in a light-sensitive pattern forming reaction using an open gel-reactor.

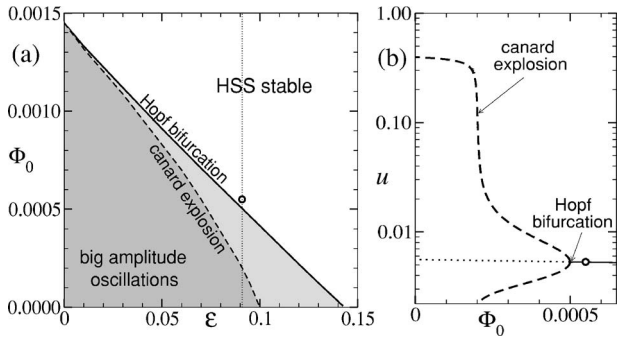


FIG. 2. (a) Stability of the homogeneous stationary state of the three-variable Oregonator model according to Eq. (1) in the $\Phi_0-\varepsilon$ parameter plane. Below the Hopf bifurcation (full line) small amplitude uniform oscillations arise (light gray area). Large amplitude relaxation oscillations (dark gray area) result from a Canard explosion (dashed line). (b) Bifurcation diagram obtained for $\varepsilon = 0.090\,91$ [the thin dotted vertical line in (a) corresponds to this $\varepsilon$ value]. The full (dotted) line indicates the stable (unstable) homogeneous stationary state. The dashed line limits the oscillation range of the $u$ variable. Small circles in (a) and (b) mark the $\Phi_0$ and $\varepsilon$ values used throughout the paper.

cillatory conditions [23,24]. Further applications of the light-sensitive BZ reaction include the study of wave dynamics in the presence of external fluctuations as, for example, noise-supported wave propagation [25], and Brownian motion of spiral waves subjected to spatiotemporal external noise [26]. Reported experimental results under global feedback include the observation of oscillatory cluster patterns [27] and the control of spiral wave dynamics in excitable domains of different shapes [28–30].

Hildebrand *et al.* have externally imposed nonlocal spatial coupling in light-sensitive BZ media through an appropriate optical feedback loop [7]. The intensity of the applied illumination in a given point of the medium has been determined by the activity in an extended neighborhood of that point. The authors reported spatial domains containing spiral waves on a stationary background which result from a nonlocal coupling with short-range activation and long-range inhibition.

A possible experimental setup for the externally imposed nonlocal spatial coupling in light-sensitive BZ media is shown schematically in Fig. 1. A continuously fed open reactor is used to maintain stationary nonequilibrium conditions. The reaction takes place in a thin gel layer where the light-sensitive catalytic complex is fixed. Details concerning the reactor and the method of gel preparation are given in [31]. The emerging concentration pattern of the oxidized form of the catalyst is detected in transmitted light by a charge-coupled device camera and digitized with a frame grabber for immediate processing by the computer. Based on the recorded data, a control signal is generated according to the specified feedback algorithm. In the video projector this signal is transformed into a corresponding space and/or time dependent intensity distribution that is applied to the gel layer. The characteristics of the feedback-mediated nonlocal coupling as, for example, the coupling function or the coupling range can be chosen arbitrarily (see below).

In this work, we study the three-variable Oregonator model with an additional integral term that takes into account a nonlocal spatial coupling as described in the schematic experimental setup. Earlier, a similar study was conducted for the two-variable Oregonator model [7], wherein a Turing instability was reported as a result of nonlocal spatial coupling. Here, the main focus is on the analysis of a wave instability in the three-variable model. Such an instability cannot be captured by the simpler two-variable model. We note that a wave instability and the resulting patterns have so far not been found experimentally in the BZ reaction in an open reactor. However, such patterns have recently been discovered in the BZ reaction in a microemulsion under batch conditions [32].

This paper is organized as follows. In the next section we present the model to be studied and specify the nonlocal spatial coupling considered in this paper. The linear stability of the steady state is discussed in Sec. III. In Sec. IV we perform a weakly nonlinear analysis and derive a set of coupled amplitude equations for the slowly varying amplitudes of the bifurcating solutions. These equations allow us to analyze the properties of the spatiotemporal patterns emerging beyond the wave instability. In Sec. V we compare our theoretical predictions with numerical simulations of the reaction-diffusion model. We conclude with a summary and a discussion of the main results.

## II. THE MODEL

In 1990, Krug *et al.* proposed an extension of the well-known Oregonator model of the BZ reaction to account for the influence of light when the light-sensitive catalytic complex $Ru(dmbpy)_3^{2+}$ is used. They assumed that under illumination the reduced form of the catalyst becomes photochemically excited and causes the release of the reaction inhibitor bromide [33]. Consequently, an additional bromide source was introduced into the bromide balance of the Oregonator model which in first approximation was considered to be proportional to the intensity of applied illumination. Let us consider this modified three-variable Oregonator model in one spatial dimension:

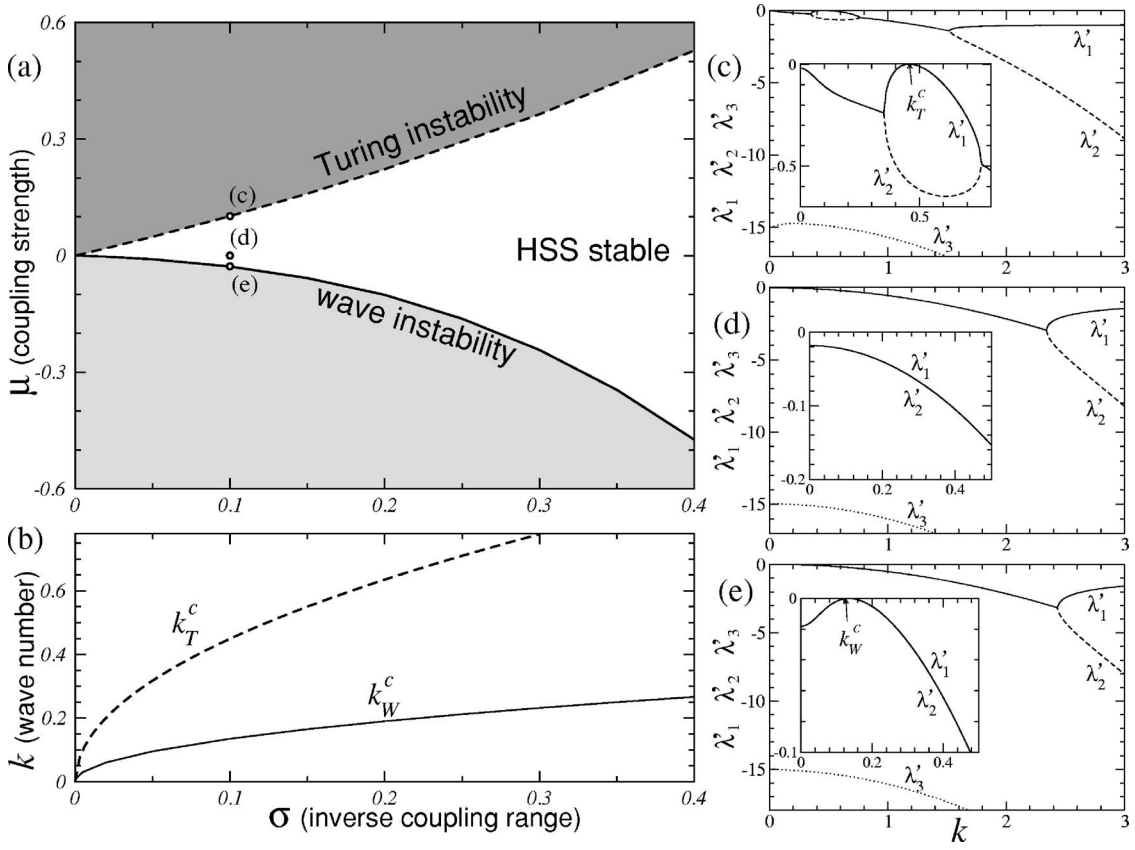


FIG. 3. Results of the linear stability analysis of the Oregonator model Eq. (1) with nonlocal spatial coupling as defined in Eqs. (2) and (3), for $\phi_0=0.000\,55$ and $\varepsilon=0.090\,91$. In (a) the instability lines are shown in the control parameter plane spanned by the inverse nonlocal coupling range $\sigma$ and the coupling strength $\mu$. The full and dashed lines correspond to the threshold for wave and Turing instability, respectively. In the white region the homogeneous stationary state is stable. The light- and dark-gray regions correspond to the locations where wave and, respectively, Turing-like patterns are expected. In (b) the critical wave numbers for the Turing ($k_T^c$) and the wave ($k_W^c$) instability are plotted as a function of the inverse coupling range $\sigma$. The dispersion relations shown in (c), (d), and (e) apply to locations marked by small circles in (a). (c) corresponds to the Turing instability, (d) to a situation where the homogeneous stationary state is stable, and (e) to the wave instability.

$$\partial_t u = \frac{1}{\varepsilon}[u - u^2 - w(u-q)] + \partial_x^2 u, \tag{1a}$$

$$\partial_t v = u - v, \tag{1b}$$

$$\partial_t w = \frac{1}{\alpha\varepsilon}[\Phi(x,t) + fv - w(u+q)] + \delta\partial_x^2 w. \tag{1c}$$

Here $u$, $v$, and $w$ are the dimensionless concentrations of $HBrO_2$, $Ru(dmbpy)_3^{2+}$ and $Br^-$, respectively. The parameter $\delta=D_w/D_u$ denotes the ratio of the diffusion constants of $w$ and $u$ (there is no diffusion in the second equation as the catalyst is fixed in the gel matrix). The characteristic time scale of $u$ is $\varepsilon$. Time scales of $u$ and $w$ depend both on the recipe concentrations and are related by a proportionality factor $\alpha$ [34,35]. Typically the bromide concentration $w$ is the fastest variable of the Oregonator kinetics and consequently $\alpha \ll 1$.

$\Phi(x,t)$ denotes the photochemically induced bromide flow. Following [33], this quantity is assumed to be proportional to the applied light intensity and consequently should be always non-negative. For the sake of simplicity, in this paper we will refer to $\Phi(x,t)$ in Eq. (1) as the light intensity. For $\Phi(x,t)\equiv 0$, the Oregonator model for the standard BZ reaction is recovered [35,36]. Following the parameter estimation done in Refs. [31,37], we choose the following parameter values $\delta=1.12$, $\alpha=0.011$, $q=0.002$, and $f=2.1$ and keep them fixed throughout this paper. In the absence of illumination these parameter values represent oscillatory conditions. The restriction to the spatially one-dimensional case allows the derivation of amplitude equations and enables systematic numerical simulations. In experiments, a quasi-one-dimensional setup can be achieved if the BZ reaction is allowed to take place in a small channel or a ring of thin width.

### A. Uniform illumination

Let us first consider the case of an illumination uniform in space and time, i.e., $\Phi(x,t)=\Phi_0=\text{const}$. This case has been discussed previously in [33]. With the parameters $\alpha$, $q$, $f$ specified above and for any value of $\Phi_0$ the model of Eq. (1) has a unique homogeneous stationary state $\boldsymbol{X}_0\equiv(u_0,v_0,w_0)$, where $u_0=u_0(\Phi_0)$ is a real solution of $u-u^2-(\Phi_0+fu)(u-q)/(u+q)=0$ with $u_0 \geqslant q$, $v_0=u_0$ and $w_0=(\Phi_0+fu_0)/(u_0+q)$.

This homogeneous stationary state undergoes a Hopf bifurcation if the control parameter $\Phi_0$ ($\propto$ light intensity) is small enough. The Hopf bifurcation in the parameter space spanned by the light intensity $\Phi_0$ and the characteristic time scale of the activator $\varepsilon$ is shown in Fig. 2(a).

After crossing the dashed line in Fig. 2(a), large amplitude relaxation oscillations emerge due to a so-called *Canard explosion* [38]. The sharp increase in the oscillation amplitude is shown in the bifurcation diagram Fig. 2(b) where the $u$ amplitude is plotted versus $\Phi_0$ on a logarithmic scale. For the chosen value of $\varepsilon$ we find uniform oscillations around the homogeneous stationary state for $\Phi_0 < 0.000\,505$. The Canard explosion takes place at $\Phi_0 \approx 0.0002$.

### B. Nonlocal spatial coupling mediated by optical feedback

Throughout this paper we consider a nonlocal coupling realized through a space-time-dependent illumination or photochemically induced bromide flow according to

$$\Phi(x,t) = \Phi_0 + \mu \int_{-\infty}^{\infty} K(y)[v(x+y,t) - v(x,t)]dy, \qquad (2)$$

where for the coupling function we choose

$$K(y) = e^{-\sigma|y|}. \qquad (3)$$

Here, $\mu$ denotes the coupling strength while $1/\sigma$ characterizes the coupling range. The sign of $\mu$ indicates whether the nonlocal spatial coupling is inhibitory ($\mu > 0$) or activatory ($\mu < 0$). In the following, we consider $\mu$ and $\sigma$ as the main control parameters.

According to Eq. (2), to determine the light intensity applied to a given point $x$ at time moment $t$ the actual difference in light transmission between that point and the other points of the medium has to be measured. This can be readily done with the experimental setup sketched in in Fig. 1. For simplicity we also neglect a time delay in the feedback loop imposed externally or possibly induced by internal latency effects. Nonlocal coupling enters into the dynamics exclusively through the actual concentration $v(x,t)$ of the oxidized form of the catalyst that is monitored experimentally. Note that the nonlocal coupling, as defined in Eq. (2), vanishes both for the homogeneous stationary state and for spatially uniform oscillations. This property is very convenient since the nonlocal term does not change the location of the homogeneous stationary state of the model. In contrast, the nonlocal coupling strongly influences the stability properties of the homogeneous stationary state as will be discussed in the next section. Recall also that only values $\Phi(x,t) \geqslant 0$ have a physical meaning.

## III. LINEAR STABILITY ANALYSIS

In this section we will consider the linear stability of the unique homogeneous stationary state with respect to spatial perturbations. Here and in the remaining part of the paper we will fix the activator time scale to $\varepsilon = 0.090\,91$ and the homogeneous light intensity, to $\Phi_0 = 0.000\,55$ [the same values as used in Fig. 2(b)].

To study the stability of the homogeneous stationary state $\boldsymbol{X}_0$ with respect to perturbations proportional to $e^{ikx-\lambda(k)t}$, we have to analyze the linear eigenvalue problem $\lambda(k)\boldsymbol{X} = \boldsymbol{J}(k)\boldsymbol{X}$. The stability matrix (Jacobian) $\boldsymbol{J}(k)$ is given by

$$J(k) = \begin{pmatrix} \dfrac{1-2u_0-w_0}{\varepsilon} - k^2 & 0 & \dfrac{-(u_0-q)}{\varepsilon} \\ 1 & -1 & 0 \\ \dfrac{-w_0}{\alpha\varepsilon} & \dfrac{\mu[2\sigma/(k^2+\sigma^2) - 2/\sigma] + f}{\alpha\varepsilon} & \dfrac{-(u_0+q)}{\alpha\varepsilon} - \delta k^2 \end{pmatrix}.$$

Eigenvalues $\lambda(k) \equiv \lambda'(k) + i\lambda''(k)$ of this matrix with a negative real part $\lambda'(k)$ indicate stability of the reference state. The dispersion relations $\lambda_1(k)$, $\lambda_2(k)$, and $\lambda_3(k)$ reveal that the homogeneous stationary state can be destabilized under nonlocal spatial coupling either by a Turing or a wave instability. Figure 3(a) shows the corresponding stability boundaries in the parameter plane spanned by the coupling strength $\mu$ and the inverse coupling range $\sigma$. While for positive values of $\mu$ a Turing instability occurs, a wave instability takes place for $\mu < 0$. In Fig. 3(c) an example of the dispersion relation of the three eigenvalues of the Jacobi matrix is plotted at the Turing instability. The threshold parameters and the critical wave number $k_T^c$ follow from the condition $\lambda_1'(k_T^c) = \lambda_1(k_T^c) = 0$ (where $\lambda_1$ denotes the dominating eigenvalue with the smallest negative real part). For the wave instability [see Fig. 3(e)], the critical value $\mu_W^c(\sigma)$ and the critical wave number $k_W^c$ are obtained from the condition $\lambda_1'(k_W^c) = 0$, where $\lambda_1''(k_W^c) = \pm\omega_0 \neq 0$. Figure 3(b) shows how the critical wave number for Turing and wave instability depend on the inverse coupling range. Both $k_W^c$ and $k_T^c$ are proportional to $\sqrt{\sigma}$. This property is very interesting because it provides a way to select an experimentally convenient wave number by changing the coupling range.

It is worth mentioning that there is no wave instability in the two-variable version of the Oregonator model with nonlocal spatial coupling that is obtained by an adiabatic elimination of the fastest variable $w$ in the Oregonator kinetics (for more details see Appendix A). Thus, in contrary to the

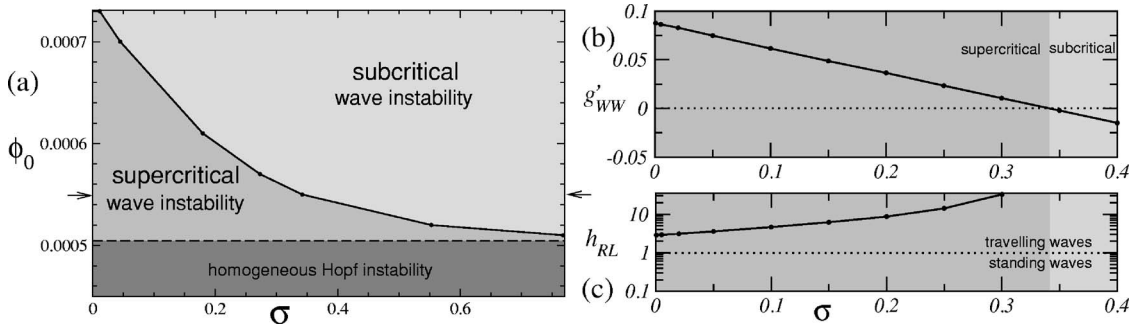


FIG. 4. Results obtained from the amplitude equations. In (a), regions in the $\Phi_0-\sigma$ parameter plane ($\varepsilon=0.090\,91$) where the wave instability is supercritical (subcritical) are indicated in middle gray (light gray). For $\Phi_0<0.000\,505$ the homogeneous stationary state undergoes a supercritical Hopf bifurcation to spatially homogeneous oscillations. This region is indicated in dark gray. In (b) and (c) the values of the real part of the coefficient $g_{WW}$ and the cross coupling coefficient $h_{RL}=g'_{RL}/g'_{WW}$ are plotted as a function of $\sigma$ for $\Phi_0=0.000\,55$ [this value of $\Phi_0$ is indicated with two arrows in (a), and corresponds to same parameter values as used in Fig. 3]. With increasing $\sigma$, the character of the wave bifurcation changes from supercritical to subcritical at $\sigma=0.3418$.

Turing instability that can be studied in the two-variable Oregonator model with nonlocal spatial coupling [7], we have to base the study of the wave instability induced by long-range spatial communication on the full three-variable model. From the experimental point of view, the latter is more realistic because it includes the diffusion of the inhibitor bromide. For these reasons in the next section our focus will be on the weakly nonlinear analysis of the wave instability in the three-variable Oregonator model with nonlocal spatial coupling Eqs. (1)–(3).

## IV. AMPLITUDE EQUATIONS FOR THE WAVE INSTABILITY

In this section, we investigate the amplitude equations in the vicinity of the wave instability. These equations can be derived using the approach developed in [39] for reaction-diffusion systems with nonlocal spatial coupling. For simplicity, in this paper we will not consider spatial modulations of the wave amplitude.

Near the wave instability, we can expand the deviations from the homogeneous stationary state in a power series with respect to the distance to the instability threshold which is assumed to be small [40,41]. More precisely, we define a small parameter $\nu$ as $\mu-\mu_W^c=\nu\gamma_1+\nu^2\gamma_2+\cdots$ and expand the fields $(u,v,w)$ with $\mathbf{X}=\mathbf{X_0}+\nu\mathbf{X_1}+\nu^2\mathbf{X_2}+\cdots$. Next, we use a multiple scale ansatz to substitute the time derivative with $\partial_t+\nu^2\partial_\tau+\cdots$, where $\tau$ is a slow time scale. We then insert these expansions in Eqs. (1)–(3) and sort the outcome in different orders of $\nu$.

The ansatz solving the lowest order equation reads

$$\boldsymbol{X}_1=[A_L(\tau)\boldsymbol{U}_W e^{i(\omega_c t+k_W^c x)}+A_R(\tau)\boldsymbol{U}_W e^{i(\omega_c t-k_W^c x)}+\text{c.c}]/2,$$

where $\boldsymbol{U}_W$ is the (complex) null eigenvector of the Jacobian $\boldsymbol{J}(k)$ at the wave instability. $A_{L,R}\in\mathbb{C}$ are the amplitudes of the left- and right-traveling waves, and c.c. stands for the complex conjugate. The solvability condition for the equation of order $\nu^2$ provides us with a set of two coupled nonlinear equations. After transforming back to the original variable $t$, these equations read

$$\partial_t A_L^\star=\eta_W A_L^\star-g_{WW}|A_L^\star|^2A_L^\star-g_{RL}|A_R^\star|^2A_L^\star, \tag{4a}$$

$$\partial_t A_R^\star=\eta_W A_R^\star-g_{WW}|A_R^\star|^2A_R^\star-g_{RL}|A_L^\star|^2A_R^\star, \tag{4b}$$

where $A_{L,R}^\star=\nu A_{L,R}$, $\eta_W\equiv(\mu-\mu_W^c)\kappa_2$ and the coefficients $\kappa_2$, $q_{WW}$, and $g_{RL}$ are complex. The general expression of these coefficients as a function of the model parameters is quite involved and not shown here.

The set of coupled amplitude equations (4) describes the slow variation of the left- and right-traveling wave amplitudes. They allow us to make some predictions about these waves and their nonlinear interactions. Indeed, from the value of the complex coefficients in front of the nonlinear terms of Eq. (4), we can gain insight into the nature of the wave instability and the properties of patterns selected near to it.

The wave instability is supercritical (subcritical) if $g'_{WW}>0$ ($g'_{WW}<0$). In Fig. 4 we plot $g_{WW}$ for different values of the homogeneous light intensity $\Phi_0$ as a function of the inverse coupling range $\sigma$. For values of $\Phi_0<0.000\,504\,5$, the system undergoes a homogeneous Hopf instability. Above this value a wave instability is possible. The $\sigma$ range for which it is supercritical decreases as $\Phi_0$ increases. A general observation is that the instability will typically become subcritical when we decrease the coupling range. In Fig. 4(b) we plot, as an example, the value of $g'_{WW}$ for $\Phi_0=0.000\,55$ showing this transition. Equations (4) allow us also to predict if either standing or traveling waves will be selected in the supercritical case $g'_{WW}>0$. If the cross coupling coefficient $h_{RL}\equiv g'_{RL}/g'_{WW}>1$, then *traveling* waves will be selected. Alternatively for $1>h_{RL}>-1$, *standing* waves will be observed. In Fig. 4(c) the value of $h_{RL}$ is plotted as a function of the inverse coupling range, for $\Phi_0=0.000\,55$. In this case, since $h_{RL}>1$, a weakly nonlinear analysis predicts that traveling waves are always preferred over standing waves.

## V. NUMERICAL SIMULATIONS OF WAVE PATTERNS

To supplement the predictions from the linear stability analysis and amplitude equations, we have performed direct

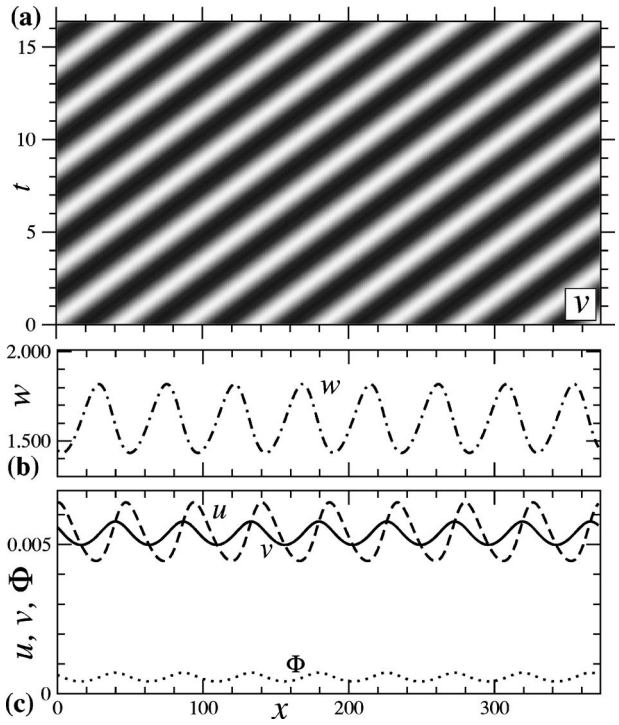


FIG. 5. Wave pattern obtained by a numerical simulation of Eqs. (1)–(3) for $\mu=-0.031$ and $\sigma=0.1$ (consequently, $\mu_W^c=-0.027\,62$ and $k_W^c=0.1349$). In (a) we show a space-time plot of $v$ with dark (light) areas representing high (low) values. The spatial profiles of $u$, $v$, $w$, and $\Phi$ are shown in (b) and (c), at the same time instant $t=16.384$ (the total integration time).

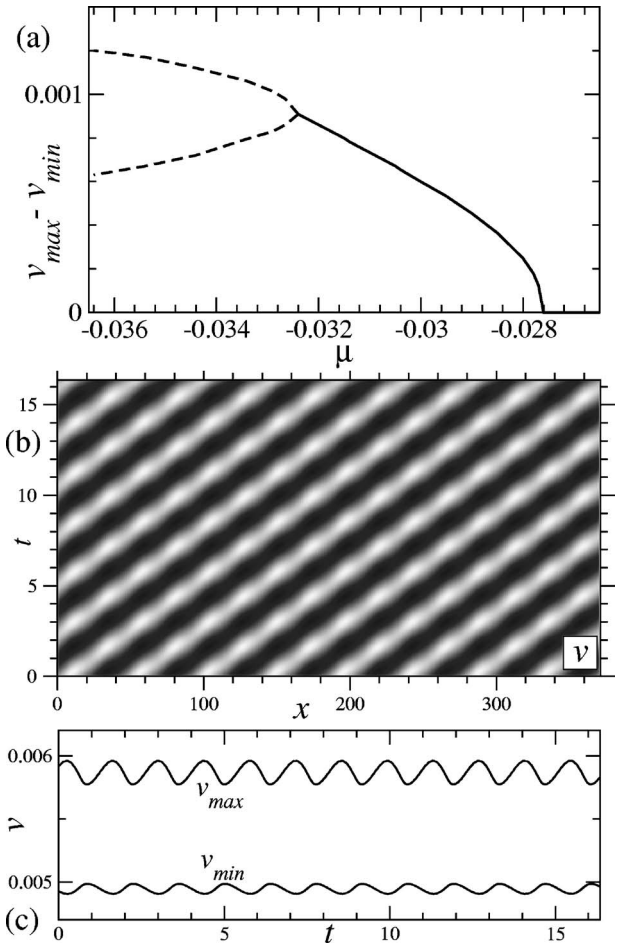


FIG. 6. (a) The full line indicates the amplitude ($v_{max}-v_{min}$) of traveling waves emerging beyond the wave instability ($\sigma=0.1$, $\Phi_0=0.000\,55$, $k=k_W^c=0.1349$). Note a secondary instability leading to modulated traveling waves. $v_{max}$ ($v_{min}$) denote the maximal (minimal) value achieved in this modulated wave pattern by the $v$ field at a given time (dashed lines). (b) Space-time plot of a modulated traveling wave obtained with a $\mu=-0.033$ wave pattern.

numerical simulations of the underlying reaction-diffusion equations Eq. (1) with nonlocal spatial coupling as defined in Eqs. (2) and (3). In all numerical simulations we have used a finite difference scheme and employed periodic boundary conditions. The outcome of the linear stability analysis is fully confirmed by these simulations. Beyond the instability thresholds, the predictions of the amplitude equations are confirmed for small amplitude patterns. However, we also find that, if the amplitude of the patterns is large, the quantity $\Phi(x,t)$ may become negative in some locations and times. A negative value of the light intensity is physically not possible. To prohibit values of $\Phi(x,t)<0$, we have replaced Eq. (2) by

$$\Phi(x,t)=\left(\Phi_0+\mu\int_{-\infty}^{\infty}K(y)[v(x+y,t)-v(x,t)]dy\right)\theta[\Phi(x,t)], \tag{5}$$

The introduced cutoff becomes relevant for patterns with larger amplitudes as will be illustrated by comparison of simulations with and without the cutoff.

In the previous section, the wave instability was predicted to be supercritical in a broad region of the parameter space. Traveling waves were found to be preferred over standing waves. These predictions are confirmed by the numerical simulations. Figure 5(a) shows a space-time plot of a right-traveling wave typically obtained near the instability threshold. Since the amplitude of the traveling wave is small [cf. Figs. 5(b) and 5(c)], $\Phi(x,t)$ remains always positive, compare the snapshot of $\Phi(x)$ in Fig. 5(c). In this case, our numerical results agree well with those obtained in the framework of the weakly nonlinear analysis. In Fig. 6(a) the amplitude of the waves is plotted as a function of the coupling strength $\mu$. The wave amplitude increases $\propto\sqrt{|\mu-\mu_W^c|}$, as predicted by the amplitude equation.

However, increasing the distance from the instability threshold, we find a secondary bifurcation for traveling waves with wave numbers close to $k_W^c$. This secondary bifurcation corresponds to a breathing of the waves width and amplitude [42]. In Fig. 6(b) a space-time plot of a modulated traveling wave is shown. From the temporal evolution of the difference between the minimum and maximum values of the wave amplitude follows [see Fig. 6(c)] that the wave amplitude changes periodically in the modulated wave pattern.

If we increase the coupling strength even further, i.e., decrease $\mu$ towards more negative values, we enter into a region where $\Phi$ can become negative. In this case we have performed numerical simulations with the described cutoff

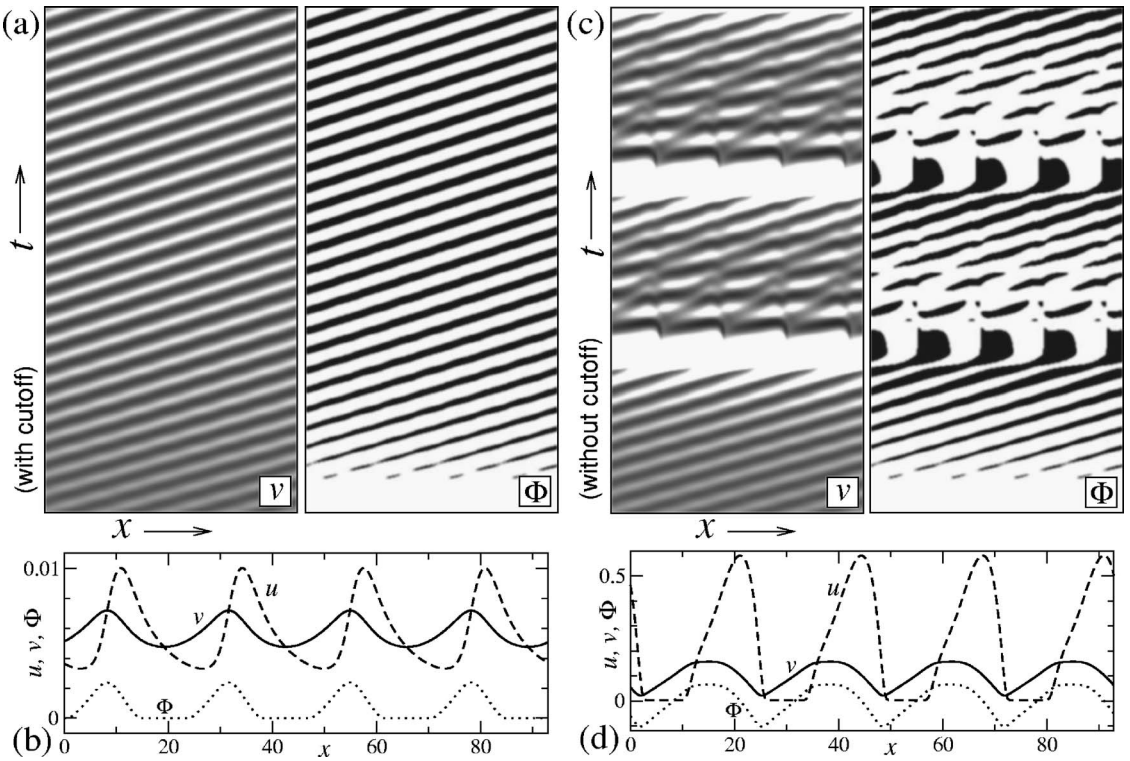


FIG. 7. Traveling wave patterns calculated numerically far from the instability threshold ($\mu=-0.07$) with a cutoff using Eq. (5) in (a) and (b) and without it using Eq. (2) in (c) and (d). Left panels in (a) and (c) show a space-time plot of $v$ in a gray-scale coding changing from dark for high to bright for low $v$ values. Right panels display $\Phi(x,t)$ with black corresponding to $\Phi(x)=0$ in (a) and $\Phi(x)\leqslant 0$ in (c) while positive $\Phi$ values are represented in white. (b) and (d) show typical spatial profiles of $u$, $v$, and $\Phi$ obtained without, respectively, with cutoff. Simulations were both started from same initial conditions, namely a small amplitude wave with wave number $k=0.2696$ (system size $L=93.2224$, total integration time $T=65.536$, $\sigma=0.1$, and $\Phi_0=0.000\,55$).

and without it. In the physical meaningful model with the cutoff, a stable traveling wave develops. The amplitude of this traveling wave is large and contains extended regions where $\Phi(x,t)=0$. An example of such a wave is shown in Figs. 7(a) and 7(b). In the simulations without cutoff the system displays a nonsteady behavior of the waves and their amplitudes. An example of this behavior is shown in Figs. 7(c) and 7(d). Initially, the wave amplitude grows until a threshold is reached where the waves collapse to very small amplitudes. After a while, new waves appear and collapse again until the cycle of growth and decay starts again. In this case, the field $\Phi$ has extended regions where it assumes unphysical negative values. Consequently, the observed behavior is an artefact of the coupling function in Eq. (2) and shows the necessity to introduce a cutoff according to Eq. (5).

## VI. CONCLUSIONS

In this paper we study a modified Oregonator model describing an experimentally feasible implementation of nonlocal spatial coupling in the BZ reaction based on an optical feedback loop. In order to explore the possible effects of this nonlocal coupling we have performed a theoretical and numerical analysis of the three-variable Oregonator model in one spatial dimension extended by an integral term representing the nonlocal coupling. While neither Turing nor wave instabilities are present in the standard Oregonator model, these instabilities can be induced in our generalized model with nonlocal spatial coupling. The wave instability is caused by a long-range activation, while the Turing instability stems from a long-range inhibition introduced by the nonlocal spatial coupling. The Turing instability had already been reported in a two-variable Oregonator model with a different type of nonlocal spatial coupling [7]. We demonstrated here that the wave instability is not reproduced by such a simpler model approach. Therefore, we have focused our study on the phenomena related to the wave bifurcation. We derived coupled equations for the temporal dynamics of the amplitudes of left- and right traveling waves and found therein parameter regimes where the wave instability is supercritical or subcritical. In the supercritical regime, the amplitude equation predicts a selection of traveling waves. These predictions have been confirmed by a numerical simulation close to the wave instability. Farther away from the threshold, a secondary instability leading to breathing traveling waves is found in the simulations. At larger distances, the illumination intensity resulting from the nonlocal spatial coupling in the model may become negative and a cutoff term has to be introduced. Numerical simulations in this regime show stable traveling waves with the cutoff and complicated dynamics without the cutoff. Altogether, our work shows that it is possible to induce a wave instability by long-range ac-

tivating nonlocal coupling and may inspire further experimental study and validations.


## ACKNOWLEDGMENTS

We would like to acknowledge preliminary work done by Gerald Kleser on the nonlocal spatial coupling. E.M.N. would like to thank financial support given by the European Commission under network Grant No. HPRN-CT-2002-00312 and by the *Sonderforschungsbereich (SFB) 555 "Komplexe nichtlineare Prozesse" (Berlin, Germany)* of Deutsche Forschungsgemeinschaft (Grant No. SFB555).


## APPENDIX A: NONLOCAL COUPLING IN THE TWO-VARIABLE OREGONATOR MODEL

In this appendix we will shortly show why a wave instability cannot be induced by a nonlocal spatial coupling in the two-variable Oregonator model. In Sec. II we pointed out that the characteristic time scale of $w$ in Eq. (1) is typically much smaller than that of $u$ (two orders of magnitude smaller for the value of $\alpha$ considered in this paper). If we further assume $\delta=0$ neglecting a diffusion of bromide, the equation for $w$ can be eliminated adiabatically

$$\partial_t u = \frac{1}{\varepsilon}\left[u - u^2 + [\Phi(x,t) + fv]\frac{q-u}{q+u}\right] + \partial_x^2 u,$$

$$\partial_t v = u - v,$$

where

$$\Phi(x,t) = \phi_0 + \mu \int_{-\infty}^{\infty} K(y)[v(x+y,t) - v(x,t)]dy$$

with an arbitrary coupling function $K(y)$.

The Jacobian of this model around a fixed point is

$$J(k) = \begin{pmatrix} a - k^2 & b(k) \\ 1 & -1 \end{pmatrix},$$

where $a \equiv [1-2u_0-2q(\Phi_0+fv_0)/(q+u_0)^2]/\varepsilon$ and $b(k) \equiv \{[\mu(\frac{2\sigma}{k^2+\sigma^2}-\frac{2}{\sigma})+f](q-u_0)/(q+u_0)\}/\varepsilon$. The eigenvalues $\lambda(k)$ can be written as $\lambda_\pm = \{\mathrm{tr}\, J \pm [(\mathrm{tr}\, J)^2 - 4\,\det J]^{1/2}\}/2$. The fixed point is stable if $\det J(k) > 0$ and $\mathrm{tr}\, J(k) < 0$ for any $k$. There are two ways in which this fixed point can become unstable; either $\det J(k) = 0$ or $\mathrm{tr}\, J(k) = 0$, for some wave number $k$. The first case corresponds to an instability of Turing type and the second to a Hopf instability. Note that in the case of a Hopf instability, the wave number with a maximal growth rate is always at $k=0$, since $\mathrm{tr}\, J(k) = a - 1 - k^2$. Therefore, the spatially homogeneous mode is the first to become unstable. Consequently, a wave instability is not possible in the two-variable Oregonator model, regardless from the parameters of the kinetics chosen or the coupling function [43]. This instability type can only be achieved with the three-variable Oregonator as discussed in this paper.


[1] M. C. Cross and P. C. Hohenberg, Rev. Mod. Phys. **65**, 851 (1993).
[2] *Chemical Waves and Patterns*, edited by R. Kapral and K. Showalter (Kluwer, Dordrecht, 1995).
[3] J. Christoph, P. Strasser, M. Eiswirth, and G. Ertl, Science **284**, 291 (1999).
[4] Y.-J. Li, J. Oslonovich, N. Mazouz, F. Plenge, K. Krischer, and G. Ertl, Science **291**, 2395 (2001).
[5] F. Plenge, H. Varela, and K. Krischer, Phys. Rev. Lett. **94**, 198301 (2005).
[6] B. Ermentrout, Rep. Prog. Phys. **61**, 353 (1998).
[7] M. Hildebrand, H. Skødt, and K. Showalter, Phys. Rev. Lett. **87**, 088303 (2001).
[8] E. M. Nicola, M. Or-Guil, W. Wolf, and M. Bär, Phys. Rev. E **65**, 055101(R) (2002).
[9] Y. Kuramoto, D. Battogtokh, and H. Nakao, Phys. Rev. Lett. **81**, 3543 (1998).
[10] P. Fronczak and J. A. Holyst, Phys. Rev. E **65**, 026219 (2002).
[11] A. Sasaki, J. Theor. Biol. **186**, 415 (1997).
[12] H. Sayama, M. A. M. de Aguiar, Y. Bar-Yam, and M. Baranger, Phys. Rev. E **65**, 051919 (2002).
[13] M. A. Fuentes, M. N. Kuperman, and V. M. Kenkre, Phys. Rev. Lett. **91**, 158104 (2003).
[14] E. Hernández-Garcia and C. López, Phys. Rev. E **70**, 016216 (2004).
[15] S. Jakubith, H. H. Rotermund, W. Engel, A. von Oertzen, and G. Ertl, Phys. Rev. Lett. **65**, 3013 (1990).
[16] M. Falcke, H. Engel, and M. Neufeld, Phys. Rev. E **52**, 763 (1995).
[17] M. Kim, M. Bertram, M. Pollmann, A. v. Oertzen, A. S. Mikhailov, H. H. Rotermund, and G. Ertl, Science **292**, 1357 (2001).
[18] A. N. Zaikin and A. M. Zhabotinsky, Nature (London) **225**, 535 (1970).
[19] A. T. Winfree, Science **175**, 634 (1972).
[20] L. Kuhnert, Nature (London) **319**, 393 (1986).
[21] O. Steinbock, V. S. Zykov, and S. C. Müler, Nature (London) **366**, 322 (1993).
[22] M. Braune and H. Engel, Chem. Phys. Lett. **211**, 534 (1993).
[23] V. Petrov, Q. Ouyang, and H. L. Swinney, Nature (London) **388**, 655 (1997).
[24] A. L. Lin, M. Bertram, K. Martinez, H. L. Swinney, A. Ardelea, and G. F. Carey, Phys. Rev. Lett. **84**, 4240 (2000).
[25] S. Kadar, J. Wang, and K. Showalter, Nature (London) **391**, 770 (1998).
[26] S. Alonso, I. Sendiña-Nadal, V. Pérez-Muñuzuri, J. M. Sancho, and F. Sagués, Phys. Rev. Lett. **87**, 078302 (2001).
[27] V. K. Vanag, L. Yang, M. Dolnik, A. M. Zhabotinsky, and I. R. Epstein, Nature (London) **406**, 389 (2000).
[28] S. Grill, V. S. Zykov, and S. C. Müller, Phys. Rev. Lett. **75**, 3368 (1995).
[29] V. S. Zykov, G. Bordiougov, H. Brandtstädter, I. Gerdes, and H. Engel, Phys. Rev. Lett. **92**, 018304 (2004).
[30] V. S. Zykov and H. Engel, Physica D **199**, 243 (2005).

[31] H. Brandtstädter, M. Braune, I. Schebesch, and H. Engel, Chem. Phys. Lett. **323**, 145 (2000).
[32] V. K. Vanag and I. R. Epstein, Phys. Rev. Lett. **87**, 228301 (2001).
[33] H.-J. Krug, L. Pohlmann, and L. Kuhnert, J. Phys. Chem. **94**, 4862 (1990).
[34] J. J. Tyson, J. Phys. Chem. **86**, 3006 (1982).
[35] J. J. Tyson, in *Oscillations and Traveling Waves in Chemical Systems*, edited by R. J. Field and M. Burger (Wiley, New York, 1985), p. 93.
[36] R. J. Field and R. M. Noyes, J. Chem. Phys. **60**, 1877 (1974).
[37] I. Schebesch and H. Engel, Phys. Rev. E **60**, 6429 (1999).
[38] M. Brons and K. Bar-Eli, J. Chem. Phys. **95**, 8706 (1991).
[39] E. M. Nicola, PhD thesis, University of Dresden, 2001 (unpublished). Available online at http://nbn-resolving.de/urn:nbn:de:swb:14-1036499969687-26395
[40] Y. Kuramoto, *Chemical Oscillations, Waves, and Turbulence* (Springer-Verlag, Berlin, 1984).
[41] G. Nicolis, *Introduction to Nonlinear Sciences* (Cambridge University Press, Cambridge, 1995).
[42] E. Schöll and D. Drasdo, Z. Phys. B: Condens. Matter **81**, 183 (1990).
[43] Note that a wave instability is possible in the two-variable Oregonator if the coupling acts also in the variable $u$ [i.e., if $a=a(k)$]. However, this could not be achieved with an optical feedback as proposed in this paper since in experiments we can only monitor the concentration of the oxidized form of the catalyst $v$.